ACS APPLIED MATERIALS & INTERFACES

Research Article

www.acsami.org

Synergistic Anticancer Activity of Photo- and Chemoresponsive Nanoformulation Based on Polylysine-Functionalized Graphene

Chunhui Wu, Qiuming He, Anni Zhu, Dan Li, Min Xu, Hong Yang, and Yiyao Liu*

Department of Biophysics, School of Life Science and Technology, University of Electronic Science and Technology of China, Chengdu, Sichuan 610054, P. R. China

Supporting Information

ABSTRACT: Multimodal therapeutic agents based on nanomaterials for cancer combination therapy have attracted increasing attention. In this report, a novel photo- and chemoactive nanohybrid was fabricated by assembling photosensitizer Zn(II)−phthalocyanine (ZnPc) and anticancer drug doxorubicin (DOX) on the biocompatible poly-L-lysine (PLL)-grafted graphene (G-PLL). This nanocomplex of G-PLL/DOX/ZnPc showed excellent physiochemical properties, including high solubility and stability in biological solutions, high drug loading efficiency, pH-triggered drug release, and ability to generalize $^1O_2$ under light excitation. Compared to free drug molecules, cells treated with G-PLL/DOX/ZnPc showed a higher cellular uptake. In particular, G-PLL/DOX/ZnPc elicited a remarkable synergistic anticancer activity owing to combined photodynamic and chemotherapeutic effects. The combination dose reduction indexes revealed that combining DOX with ZnPc provided strong synergistic effects (combination index < 0.1) against three cancer cell lines tested (HeLa, MCF-7, and B16). Thus, this study demonstrates programmable dual-modality therapy exemplified by G-PLL/DOX/ZnPc to synergistically treat cancers.

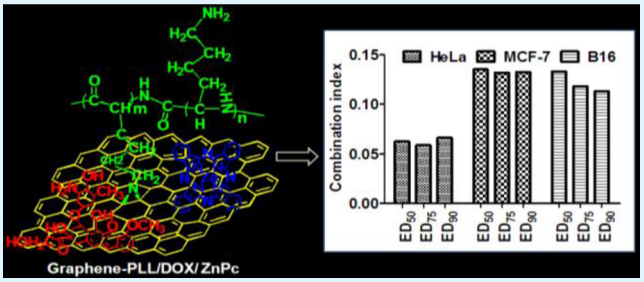

KEYWORDS: *poly-L-lysine-functionalized graphene, photosensitizer, chemotherapy, photodynamic therapy, synergistic anticancer efficiency*

INTRODUCTION

Currently, multimodal anticancer nanomedicine is attracting enormous interest due to its advantages such as targeting, signaling different cancerous pathways, synergizing/combining therapeutic outcome, and reducing undesirable side effects (e.g., drug resistance) of the individual conventional therapy technique.[1−3] Photodynamic therapy (PDT), a type of noninvasive phototherapy, utilizes highly reactive oxygen species (such as $^1O_2$) generated from a photosensitizer (PS) under the appropriate light irradiation to kill cancer cells.[4,5] PDT selectively destroys tumors without damaging adjacent healthy tissues, and repeated treatment is possible without initiating resistance. However, many of the commonly used PSs are hydrophobic in nature and not water soluble, thus seriously limiting PDT effects. Also, the inability of light to sufficiently reach deep tumors in the body remains another major obstacle of PDT.[6] Given these disadvantages of PDT, more attention is currently focused on combining PS with chemotherapeutic drug,[7] genes,[8,9] photothermal agent,[10−12] imaging probe,[13,14] etc., into one nanosystem to establish a multifunction platform to enhance anticancer performance. For example, it has been reported that PSs loaded on various plasmonic gold nanoparticles (such nanoshell,[3] hollow nanospheres,[8,9] nanorods,[10] nanocages,[11]) showed significant synergistic in vitro and in vivo photothermal therapy and PDT anticancer effect. Recently, a new therapeutic modality termed PhotoImmunoNanoTherapy was proposed based on the PS-loaded calcium phosphosilicatenanoparticles[15] or integrating PS with immune-stimulant CpG oligodeoxynucleotides,[16] which result in the significant PDT-induced immunotherapeutic response of malignant metastatic cancers. Thus, combining PDT and other techniques into one system is a promising strategy to achieve enhanced therapeutic outcome.

Graphene, an important member of a carbon nonmaterial, is being widely investigated for its promising applications in biological and biomedical areas.[17] It had been well demonstrated as a highly efficient carrier of aromatic drugs (e.g., DOX[18]) and various hydrophobic PS molecules, such as chlorin e6 (Ce6),[19−21] hypocrellin A,[22] and hypocrellin B[23] due to their unique sheet-like structure, high surface area, stability in aqueous solution, and minimum cytotoxicity. In particular, functionalized graphene shows great potential to delivering multidrugs,[24] targeting ligand,[25] and imaging agent[26] for cancer therapy and diagnosis. For instance, complexes of polyethylene glycol-grafted graphene oxide with Ce6 and DOX have recently been demonstrated to have a significantly increased tumor tissue distribution and enhanced synergistic chemotherapeutics and PDT effects in tumor-bearing mice.[27] Moreover, function-

Received: September 26, 2014
Accepted: November 5, 2014
Published: November 5, 2014

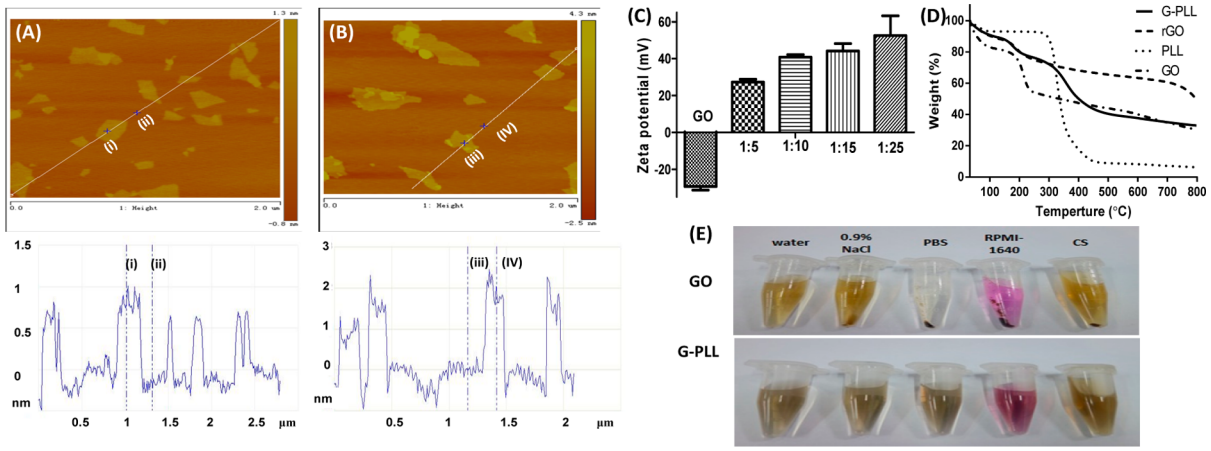

Figure 1. (Left) AFM images of GO (A) and G-PLL (B) and the topographic height of GO and G-PLL. (Right) Zeta potential of G-PLL at different ratios of [GO]/[PLL] (C) and TGA curves of PLL, GO, rGO, and G-PLL (D) and digital image of GO and G-PLL (0.2 mg/mL) dispersed in water, 0.9% NaCl, PBS, cell culture medium, or pure calf serum (CS) after centrifugation (10 000*g*, 5 min) (E).

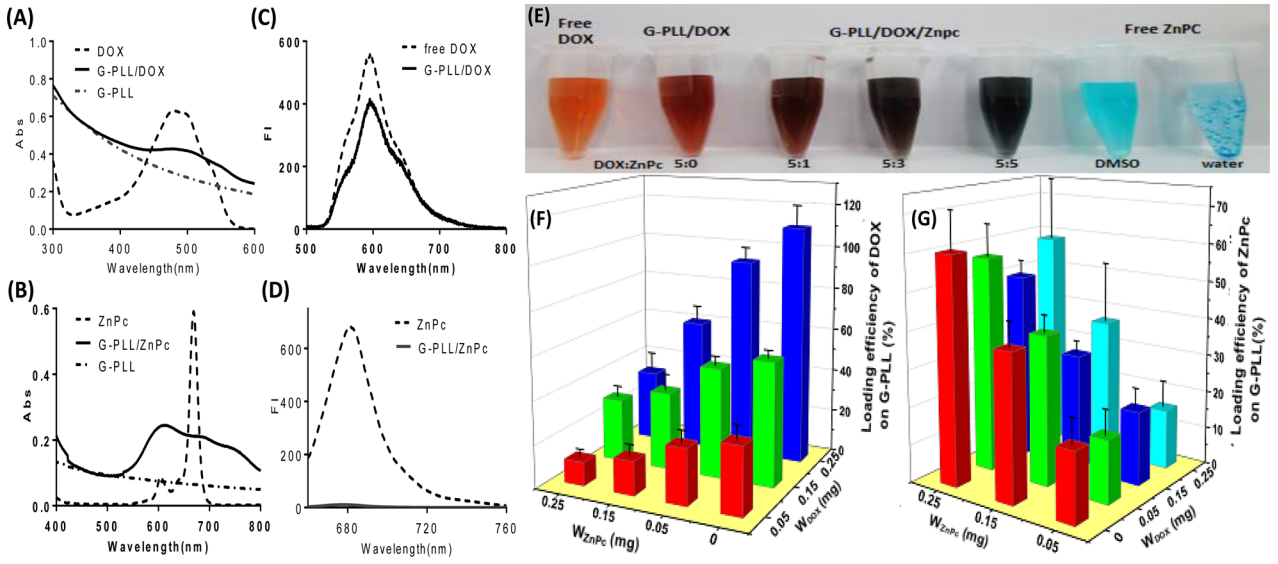

Figure 2. UV−vis absorption spectra of free DOX (90 μM), G-PLL, and G-PLL/DOX in water (A) and free ZnPc (40 μM, in DMF), G-PLL, and G-PLL/ZnPc in aqueous solution (B). Fluorescence spectra for DOX and G-PLL/DOX (90 μM, in water, C) and ZnPc (40 μM, in DMF) and G-PLL/ZnPc (40 μM, in water containing 5% DMF, D). (E) Optical photos of free DOX, free ZnPc, G-PLL/DOX, and G-PLL/DOX/ZnPc. Loading efficiency of DOX (F) and ZnPc (G) on G-PLL ($W_{G\text{-}PLL}$ = 0.05 mg) when coloaded with the two drugs at different ratios.

alized graphene has been demonstrated to be a promising platform in the combined treatment of PDT and photothermal therapy.[28,29]

Polymer poly-L-lysine (PLL) has good biocompatibility, multiple functional amino groups, a flexible molecular backbone, and excellent solubility in water. It has been utilized as a "friendly" matrix to immobilize bioactive molecules[30] and cells. Moreover, modifying nanomaterials (e.g., single-walled carbon nanotube) with PLL can reduce their toxicity.[31,32] Lee and coworkers first found that composites of PLL with graphene oxide (GO) and reduced GO can provide potent antibacterial activity but without cytotoxicity on human cells.[33] Moreover, it was reported that PLL-functionalized uniform small GO-CpG showed higher immunostimulatory activity than azide-functionalized counterpart.[34]

In this work, we aim to fabricate a novel photo- and chemoresponsive nanoformulation based on poly-L-lysine-functionalized graphene and explore its potential applications for combination therapy. The nanosized PLL-functionalized graphene (G-PLL) was first synthesized and then formed a complex with both hydrophilic DOX and hydrophobic Zinc(II) phthalocyanine (ZnPc, a second-generation PS) to generate the dual-drug nanocomplex. The physical behaviors (including the solubility, stability, drug loading capacity, and release profiles), generation of singlet oxygen, cellular uptake and distribution, synergistic anticancer efficiency toward three kinds of cancer cells (HeLa, MCF-7, and B16), and initialization mechanism were evaluated. Our results demonstrated that the multifunctional nanoparticles based on polymer-functionalized graphene (G-PLL/DOX/ZnPc) afforded highly potent antitumor activity, thus providing insight into potential biomedical applications of functionalized graphene composites.

RESULTS AND DISCUSSION

Synthesis and Characterization of Nanosized G-PLL Composite. G-PLL was synthesized through reaction of the epoxy groups on GO and the amino groups of PLL. Formation of G-PLL complexes was confirmed by UV−vis absorption

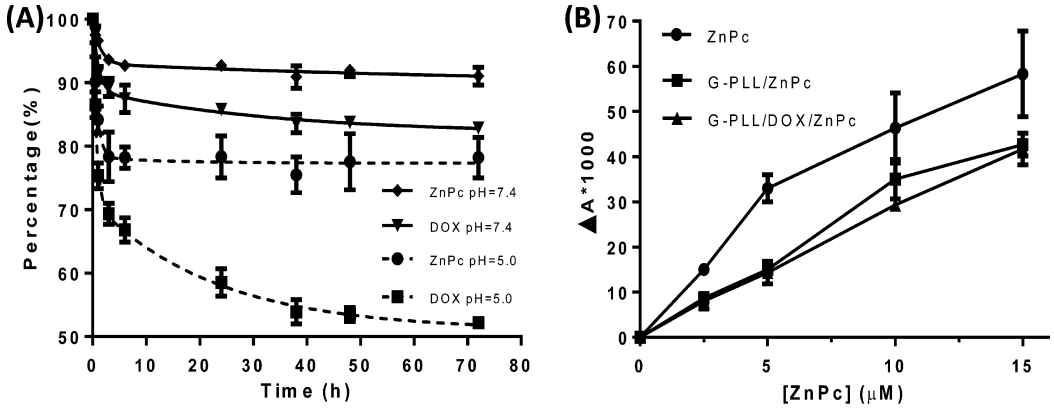

Figure 3. (A) Release curves of DOX and ZnPc in PBS buffer (pH = 5.0 and 7.4). (B) Decrease of absorbance at 440 nm of $^1O_2$ probe when incubated with ZnPc, G-PLL/ZnPc, and G-PLL/DOX/ZnPc under irradiation.

spectra, FTIR, and XPS (Figure S1, Supporting Information). The lateral dimension of single-layered G-PLL was similar to that of GO sheets (ca. 200 nm), but the thickness grew from 1.0 to 2.0 nm as observed from the representative AFM images (Figure 1A and 1B). G-PLL bared positive charge, and the zeta potential value varied with the ratio of [GO]/[PLL]. When [GO]/[PLL] = 1:5 (Figure 1C), the zeta potential was 27.3 ± 1.1 mV (zeta potential for GO is −29.3 ± 0.6 mV), and we chose this ratio in subsequent studies. Thermogravimetric analysis (TGA) was performed to assess the amount of conjugated PLL. As can we see from Figure 1D, G-PLL had three stages of weight loss and the initial two stages were similar to that of GO[35] but at less weight loss scale (ca.10% H_2O and ca. 20% oxygen-containing groups), and then a relatively large mass loss (ca.30%) was observed from 300 to 500 °C, which was attributed to the PLL decomposition. The approximate amount of PLL in G-PLL was estimated to be about 33.3% according to the TGA traces.

G-PLL exhibited well dispersion and stability in various biological solutions, including water, 0.9% NaCl, PBS, RPMI-1640 cell culture medium, and pure calf serum (CS). Even after high-speed centrifugation (10 000*g*, 5 min), no sign of aggregation and precipitation was observed (Figure 1E), whereas GO was only well dispersed in water but extensively aggregated in the other four solutions. The results suggested that G-PLL could sustain the electrostatic charges and nonspecific binding of proteins. We also found that the G-PLL solution is still stable after 3 months placement (data not shown). The cationic PLL-stabilized graphene shows similar physical property to those functionalized with hyaluronic acid,[21] branched polyethylene glycol,[27,36] polyvinylpyrrolidone,[37] and poly(ether imide).[38] Thus, PLL could be an alternative polymer to functionalize graphene sheets for biological applications, for instance, as a vector to delivery of anticancer drug for cancer therapy.

Fabrication of Chemo- and Photoresponsive G-PLL/DOX/ZnPc Formulation. In order to fabricate the chemo- and photoactive G-PLL/DOX/ZnPc formulation, we first investigated the binding behaviors of anticancer drug DOX and water-insoluble hydrophobic ZnPc to G-PLL. Complexes G-PLL/DOX (Figure 2A) and G-PLL/ZnPc (Figure 2B) clearly showed the characteristic absorption peak of DOX and ZnPc, respectively, with the peak red shifted which was probably due to the ground-state electron donor−acceptor interaction between G-PLL and the two drugs.[18,39,40] However, from the fluorescence spectrum, a different degree of fluorescence intensity (FI) quenching for DOX and ZnPc emission peak was observed (Figure 2C and 2D). The maximum FI of G-PLL/DOX only decreased about 25%, which was different from the reported results of significant quenching of FI by GO because of a photoinduced electron-transfer process or energy transfer along the GO interface,[18,36] while for G-PLL/ZnPc FI was decreased dramatically. These phenomena might suggest different binding behaviors for DOX and ZnPc on G-PLL. The hydrophobic and planar ZnPc directly absorbed on the sp^2-hybridized aromatic network of a graphene sheet through $\pi-\pi$ interaction and/or hydrophobic interaction. For DOX, the quinone portion not only can form a $\pi-\pi$ stacking interaction with the large π-conjugated structure of G-PLL but also the −OH, −O−, and −COOH groups can form hydrogen-bond and/or electrostatic interaction with NH_2 groups of G-PLL.

G-PLL/DOX/ZnPc can be easily constructed by self-assembling ZnPc and DOX on G-PLL, and clear brown to purple solutions were seen at ratios of [DOX]/[ZnPc] from 5:1 to 5:5 (Figure 2E). The characteristic absorption peaks and fluorescence emission peaks of DOX and ZnPc can be easily observed for the complex of G-PLL/DOX/ZnPc (Figure S2, Supporting Information). As presented in Figure 2F, it was found that the loading efficiency (by weight) of DOX on G-PLL ($W_{G\text{-}PLL}$= 0.05 mg) decreased with increasing amount of ZnPc. For example, the loading capacity of DOX (feeding amount equals 0.25 mg) is nearly 90% when the feeding amount of ZnPc is 0.05 mg; however, it decreased to ca. 30% when ZnPc amount is 0.25 mg. In contrast, the loading efficiency of ZnPc was not affected by DOX (Figure 2G). The efficiency could reach ca. 60% when ZnPc (0.25 mg) was fed with a different amount of DOX (0−0.25 mg). These phenomena may result from the different interaction between G-PLL and DOX/ZnPc. We speculate that the binding of ZnPc onto G-PLL was driven by hydrophobic interactions and $\pi-\pi$ stacking between ZnPc and aromatic regions of the graphene sheets. However, for DOX, besides the $\pi-\pi$ stacking interaction, hydrogen-bonding and/or electrostatic interaction also was the driving force. The noncovalent ZnPc and G-PLL are much stronger in nature than that of DOX, so ZnPc may greatly compete with the binding of DOX, but the later exert little effect on the former. G-PLL/DOX/ZnPc formulation showed good solubility and stability in water, 0.9% NaCl, PBS, RPMI-1640 cell culture medium, and CS solution at

concentrations up to ~0.1 mg/mL (Figure S3, Supporting Information).

G-PLL/DOX/ZnPc showed pH-dependent drug release profiles (Figure 3A), which may be an advantage because the intracellular microenvironments in tumors are acidic in nature.[41] At pH = 7.4, only 15% of loaded DOX was released within 72 h incubation. However, at pH = 5.0, more than 35% of DOX was released at the initial 6 h and increased to almost 48% after 72 h. The release rate of ZnPc was much slower than that of DOX, and about 10% and 22% was released in 6 h incubation at pH = 7.4 and 5.0, respectively. Then it plateaued after 24 h incubation. This different release phenomenon can be explained as follows. The amphiphilic PLL has plenty of amino groups and became protonated with decreasing pH, thus precluding strongly with positively charged DOX molecules, leading to the faster release of DOX molecules from G-PLL. Additionally, the DOX molecule has a functional NH_2 group, so its hydrophilicity becomes higher than that of hydrophobic ZnPc under acidic conditions.

Generation of $^1O_2$ for G-PLL/DOX/ZnPc was detected using a *p*-nitrosodimethylaniline (RNO) probe, whose absorbance at 440 nm would be diminished in the presence of $^1O_2$.[42] From Figure 3B it can be seen that the $^1O_2$ generation ability of G-PLL/DOX/ZnPc and G-PLL/ZnPc was similar. Thus, the presence of DOX had no effect on the photochemistry of ZnPc. $^1O_2$ generation of G-PLL/ZnPc and G-PLL/DOX/ZnPc was much lower than that of free ZnPc. A similar quenching effect of $^1O_2$ production from PS loaded onto nanomaterials (e.g., GO[19] and carbon nanotubes[43]) was observed, and the activity of PS can be restored once released,[11,19] thus allowing use for PDT treatment of cancer cells.

Microscopic Analysis of Cellular Uptake and Intracellular Distribution of G-PLL/DOX/ZnPc. We then evaluated the cellular uptake and intracellular distribution of G-PLL/DOX/ZnPc (Figure 4). The nucleus was stained with the specific fluorescent probe DAPI. Cells treated with G-PLL/DOX displayed an intense homogeneous green fluorescence in both cytoplasm and the nucleus, while for the group treated with G-PLL/ZnPc only red fluorescence was observed from the cytoplasm, indicating that ZnPc was released from G-PLL in the cells and thereby recovering its own fluorescence. Strong intracellular yellow fluorescence from the overlapped images was observed in the cytoplasm for the group treated with G-PLL/DOX/ZnPc, proving abundant DOX/ZnPc was colocalized in the cytoplasm. The fluorescence distribution in cells was possibly owing to the endocytosis of G-PLL/DOX/ZnPc by cells. It can be easily speculated that G-PLL may have high affinity to cell membrane and can easily enter into cells (e.g., via endocytosis[36]) and shuttles ZnPc and DOX into cells. Thus, it could be predicted that G-PLL/DOX/ZnPc has potential as a nanodrug in PDT as well as chemotherapy.

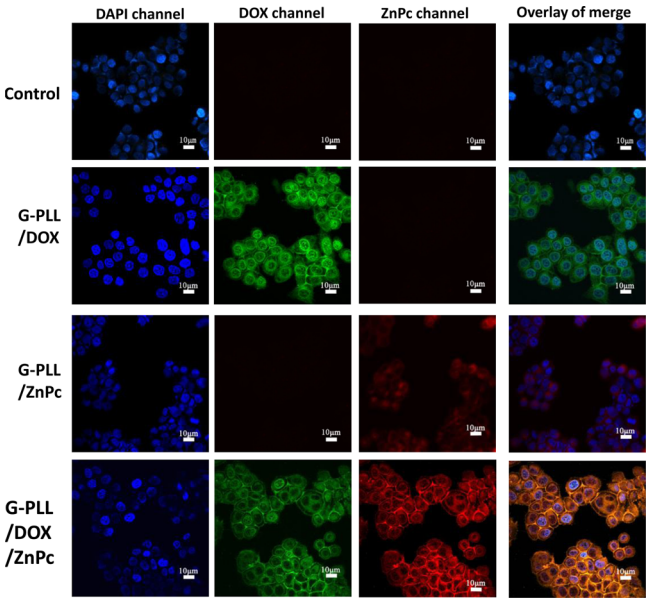

Figure 4. Confocal fluorescence microscope images of HeLa cells incubated with G-PLL/DOX, G-PLL/ZnPc, and G-PLL/DOX/ZnPc (5 μg/mL) for 6 h.

In Vitro Synergistic Efficiency of PDT and Chemotherapy of G-PLL/DOX/ZnPc. The cytotoxicity of G-PLL and G-PLL/DOX, G-PLL/ZnPc was evaluated by the cell counting kit-8 assay.[44,45] Plain G-PLL showed nontoxicity toward HeLa cells after 72 h incubation either in the dark or under irradiation, indicating the good biocompatibility of G-PLL as a nanovector (Figure S4, Supporting Information). DOX exhibited much higher cytotoxicity than that of G-PLL/DOX toward HeLa cells with an IC_{50} value of 2.63 μg/mL. IC_{50} for G-PLL/DOX decreased to 6.19 μg/mL (24 h), suggesting that DOX was slowly released from G-PLL/DOX. Of note, irradiation did not affect the cytotoxicity of DOX (Figure 5A and 5B). The cytotoxicity of ZnPc and G-PLL/ZnPc on HeLa cells was negligible in the dark at concentrations of ZnPc ranging from 0.625 to 10 μg/mL; more than 85% of cells were viable at the maximum concentration of ZnPc (10 μg/mL). Upon irradiation (0.15 W/cm^2, 10 min), significant cytotoxicity was observed, especially at higher concentrations (Figure 5C), resulting in IC_{50} of 3.52 μg/mL (24 h incubation time). For the control, a laser did not cause any photodamage to the cells in the absence of G-PLL or ZnPc.

To explore the in-vitro synergistic anticancer efficiency, HeLa cells were treated with G-PLL/DOX/ZnPc both in the dark and under irradiation. As shown in Figure 6A, G-PLL/DOX/ZnPc exerted considerable anticancer activity in the dark, which was due to the toxicity of DOX. However, when subjected to irradiation, dramatically enhanced cell-killing efficiency at a concentration range from 0.078 to 5 μg/mL was observed. For example, G-PLL/DOX/ZnPc ([DOX] = [ZnPc] = 0.625 μg/mL) caused approximately 90% loss of cell viability upon irradiation. The IC_{50} of G-PLL/DOX/ZnPc ([G-PLL]:[ZnPc]:[DOX] = 1:3:3 in weight ratio) for DOX/ZnPc was 0.14 μg equivalent DOX/ZnPc/mL.

Moreover, we utilized the combination index (CI) to evaluate the synergism via the Chou−Talalay method, a widely used approach for assessment of pharmacodynamic drug interactions.[46] CI could be calculated according to the following equation

$$\mathrm{CI} = \frac{D_{\mathrm{A|A+B}}}{D_{\mathrm{A}}} + \frac{D_{\mathrm{B|A+B}}}{D_{\mathrm{B}}} \quad (1)$$

where $D_{\mathrm{A|A+B}}$ and $D_{\mathrm{B|A+B}}$ is the dose for DOX and ZnPc in G-PLL/DOX/ZnPc, which has a 50%, 75%, or 95% cancer cell-killing effect, D_{A} is the dose for DOX in G-PLL/DOX, which has a 50%, 75%, or 95% cancer cell-killing effect, and D_{B} is the dose for ZnPc in G-PLL/ZnPc, which has a 50%, 75%, or 95% cancer cell-killing effect. The CI value reflects the interaction

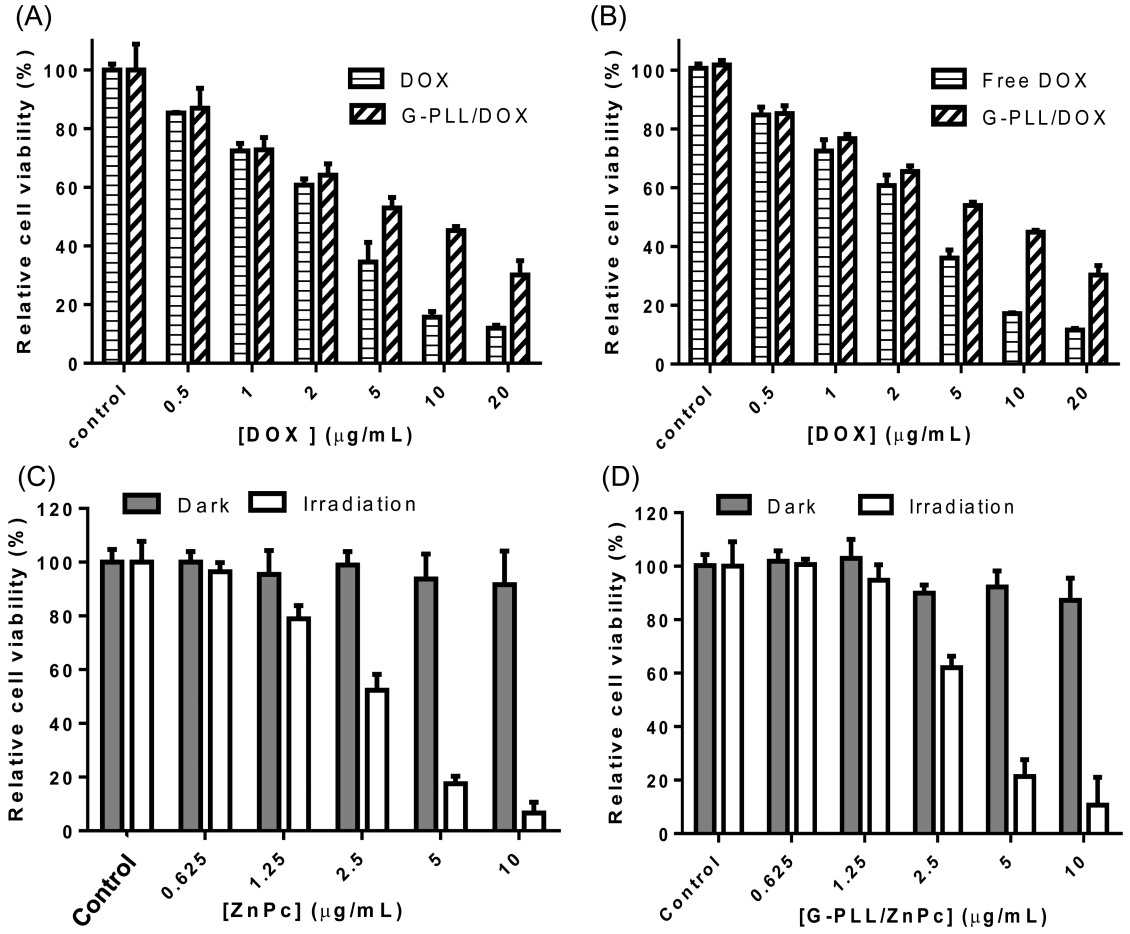

Figure 5. Relative cell viability of HeLa cells incubated with free DOX and G-PLL/DOX in the dark (A) and under irradiation (B) and free ZnPc (C) and G-PLL/ZnPc (D) in the dark and under irradiation.

effect of the dual drugs. CI > 1 indicates an antagonism effect; CI = 1 indicates an additive effect; CI < 0.1 indicates very strong synergism; 0.1 < CI < 0.3 indicates strong synergism; 0.3 < CI < 0.7 indicates synergism; 0.7 < CI < 0.85 indicates moderate synergism; 0.85 < CI < 0.9 indicates slight synergism.[46] As shown in Figure 6B, the CI values at effective dose (ED) ED_{50}, ED_{75}, and ED_{90} were <0.1, indicating that a very strong synergistic effect can be obtained after exposure of HeLa cells to G-PLL/DOX/ZnPc after 24 h treatment. Importantly, such high synergistic anticancer effect of G-PLL/DOX/ZnPc was also observed with two other cancer cell lines, human breast cancer cells MCF-7 and mouse melanoma B16 cells (Table 1). These data clearly confirmed that the nanodrug of G-PLL/DOX/ZnPc had a potent synergistic effect of PDT and chemotherapy modalities.

The trypan blue assay was further utilized to confirm the anticancer synergism of G-PLL/DOX/ZnPc (Figure 6C–F). Compared with the control and single-treatment group of G-PLL/DOX or G-PLL/ZnPc, more dead cells (blue) for the group of G-PLL/DOX/ZnPc treatment were observed. Thus, the cell viability dramatically decreased when cells were treated with G-PLL/DOX/ZnPc nanocomposite, which could synergistically kill cells through both PDT and chemotherapy.

Synergistic Anticancer Mechanism of G-PLL/DOX/ZnPc. Taken together, our study demonstrated that PLL-grafted GO can act as a new type of codelivery vehicle for anticancer drugs and photosensitizers. In addition, the obtained novel photo- and chemoresponsive architecture G-PLL/DOX/ZnPc showed remarkable synergism of chemotherapy and PDT compared with a single treatment. Relevant mechanisms may be explained in Scheme 1. First, G-PLL derivatives served as an excellent carrier to deliver anticancer DOX and hydrophobic ZnPc molecules via $\pi-\pi$ stacking interactions, hydrophobic interactions, hydrogen bonding, etc. DOX and ZnPc could be loaded on G-PLL with high payload (Figure 2). Second, G-PLL derivatives could simultaneously deliver its multiple therapeutic payloads, i.e., ZnPc and DOX, to cancer cells as observed from the confocal microscopic studies (Figure 4), probably via the endocytosis pathway.[36] Third, G-PLL/DOX/ZnPc showed pH-dependent release of both drugs, which was much faster in an acidic than in a neutral environment (Figure 3). This would favor intracellular release of drugs and generation of $^1O_2$ inside a cell to oxidize the cellular compartments. Generation of $^1O_2$ in intracellular compartments is important because the lifetime of ROS is usually short. For example, the lifetime of $^1O_2$ is only 1 μs in aqueous solution, and during such an interval it can diffuse over a mean radial distance of only 100 nm.[47,48] Fourth, combined with the anticancer activity of DOX, a synergistic effect of chemotherapy and PDT could be obtained after exposure of the cancer cells to G-PLL/DOX/ZnPc together with irradiation (Figure 6 and Table 1). Consequently, the combined G-PLL/DOX/ZnPc system allowed us to adjust and reduce the dose of each drug to maximize therapeutic efficacy.

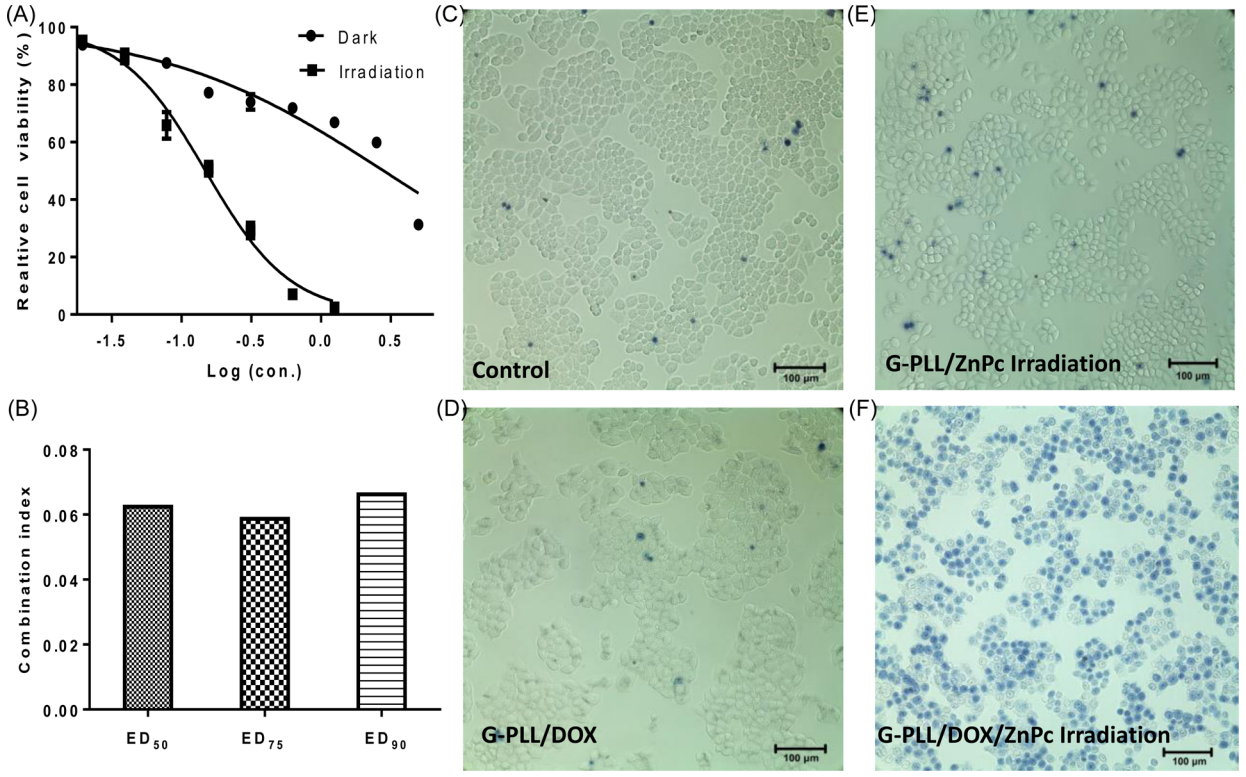

Figure 6. Synergistic anticancer effect of G-PLL/DOX/ZnPc. (A) HeLa cells were treated with G-PLL/DOX/ZnPc ([G-PLL]:[ZnPc]:[DOX] = 1:3:3 in weight ratio) in the dark and under irradiation. (B) Combination index values were calculated for ED_{50}, ED_{75}, and ED_{90} based on the dose–response curves of ZnPc and DOX. (C–F) Representative optical images of HeLa cell stained with trypan blue for the control (untreated cells, C) and cells treated with G-PLL/DOX (D), G-PLL/ZnPc (E), and G-PLL/DOX/ZnPc (F).

Table 1. IC_{50} (μg/mL) of G-PLL/DOX/ZnPc under Irradiation Toward the HeLa, MCF-7, and B16 Cancer Cells and CI Values @ ED_{50}, ED_{75}, and ED_{90}

cell	G-PLL/DOX	G-PLL/ZnPc	G-PLL/DOX/ZnPc	CI@ ED_{50}	CI@ ED_{75}	CI@ ED_{90}
HeLa	6.19	3.52	0.14	0.062	0.059	0.066
MCF-7	2.49	4.07	0.21	0.135	0.132	0.132
B16	3.96	4.61	0.28	0.133	0.118	0.113

Scheme 1. Proposed Syngerstic Anticancer Mechanism of G-PLL/DOX/ZnPc

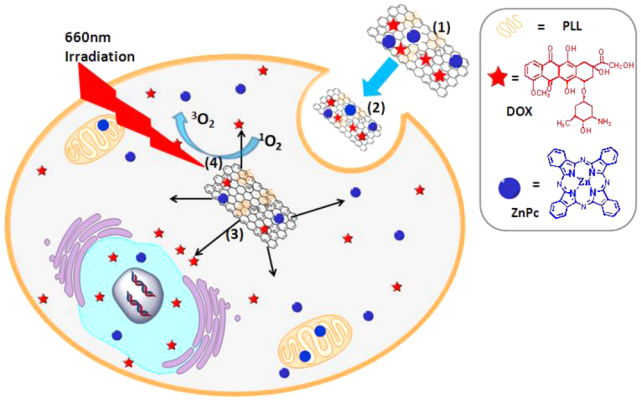

CONCLUSION

In summary, a novel photo- and chemoactive nanodrug of G-PLL/DOX/ZnPc was fabricated based on the biocompatible nanosized PLL-functionalized graphene nanocomposites. The cellular uptake and trafficking, in vitro PDT, and chemotherapy efficacy were evaluated using three cancer cell lines. G-PLL/DOX/ZnPc displayed high stability, high drug loading efficiency, and high $^1O_2$ yield for PDT. G-PLL/DOX/ZnPc can simultaneously and efficiently deliver ZnPc and DOX to the cytoplasm and cell nucleus, probably by endocytosis. In particular, in-vitro biological assays demonstrated that high synergistic PDT and chemotherapy efficiency could be achieved in combination with light irradiation. This study highlights the promising applications of nanomedicine based on graphene derivatives for cancer combination therapy. Further studies evaluating the biodistribution and antitumor activity of combined PDT and chemotherapy in preclinical tumor xenograft models are warranted.

EXPERIMENTAL SECTION

Materials. Poly-L-lysine hydrobromide (PLL, M_w = 30 000–70 000), zinc(II) phthalocyanine (ZnPc), and doxorubicin hydrochloride (DOX) were obtained from Sigma-Aldrich (St Louis, MO, USA). *p*-Nitrosodimethylaniline (RNO) was obtained from Alfa Aesar. GO stock solution was purchased from XFNano Co., Ltd. (Nanjing, China). All other reagents were of analytical grade and used as received. Aqueous solutions were prepared with double-distilled water from a Millipore system (>18 MΩ cm).

Synthesis and Characterization of G-PLL. GO stock solution was first ultrasonicated by a probe for 2 h (Φ6, 35% amplitude, scientz-IID) to obtain the nanosized GO. Then GO was reacted with PLL according to the literature with minor modification.[30] Two milliliters of GO solution (0.5 mg/mL) was diluted with KOH solution (pH = 9) to 4 mL, mixed with PLL (5 mg), and adjusted to pH = 9.0 with KOH solution (pH = 11). The solution was stirred at 70 °C for an additional 24 h, and the G-PLL nanoparticles were collected and purified by centrifugation 3 times at 15 000 rpm for 30

min and concentrated with 100 kDa ultra film. The morphology of G-PLL was characterized using atomic force microscope (AFM, Veeco Dimension 3100, USA). UV−vis spectra were measured with Hitachi U-2910 (Hitachi, Japan), and fluorescence spectra were recorded on a Hitachi F-7000 fluorescence spectrophotometer (Hitachi, Japan). Fourier transform infrared spectroscopy (FTIR) was recorded using a Nicolet NEXUS 670 (Thermo, America). X-ray photoelectron spectroscopy (XPS) analysis was carried out on an XSAM-800 (KRATOS, UK) with Al Kα radiation. Zeta potential was detected using a Zeta Potential Analyzer (Brookhaven, ZetaPALS, USA).

For the stability studies G-PLL was dissolved in water, 0.9% NaCl saline, phosphate-buffered saline (PBS), RPMI1640 cell culture medium, or pure calf serum (CS). All solutions were centrifuged at 10 000g for 5 min.

Loading of ZnPc and DOX on G-PLL. A 100 μL amount of G-PLL aqueous solution (0.5 mg/mL) was mixed with 50, 150, and 250 μL of ZnPc (1 mg/mL in DMSO) or DOX (1 mg/mL in water) or different mixtures of DOX and ZnPc (at weight ratios of 1:1, 1:3, 1:5, 3:1, 3:3, 3:5, 5:1, 5:3, 5:5) and then diluted to 2 mL with PBS (pH = 9, 10 mM). Mixtures were shaken (200 rpm) on a platform shaker (ZHWY-103D, ZhiCheng Inc., Shanghai) for 12 h at 25 °C. The obtained G-PLL/ZnPc, G-PLL/DOX, or G-PLL/DOX/ZnPc complex was collected by centrifugation at 13 000 rpm for 15 min and washed with ultrapure water 3 times. The resulting complex was dissolved in 100 μL of water before use. The loading capability of ZnPc or DOX on G-PLL was determined by UV−vis absorption spectroscopy (604 nm for ZnPc, 480 nm for DOX) and calculated according to the following equation: Drug loading capability (%) = $(W_{feeded} - W_{residual})/W_{G\text{-}PLL} \times 100\%$ (2), where W_{feeded} was the weight of initial drug for loading, $W_{residual}$ was the weight of residual drug in solution after loading, and $W_{G\text{-}PLL}$ was the total weight of G-PLL for loading. The fluorescence spectrum for G-PLL/ZnPc or G-PLL/DOX or free DOX (λ_{ex}= 480 nm) was measured in aqueous solution, and free ZnPc was determined in DMF (λ_{ex} = 600 nm).

Release Profiles of G-PLL/DOX/ZnPc. The G-PLL/DOX/ZnPc solution was diluted in PBS (pH = 7.4 and 5.0) and shaken (180 rpm) on a platform shaker at 37 °C for 1, 3, 6, 24, 36, 48, and 72 h. At each time point the samples were centrifuged at 13 000 rpm for 15 min, and the precipitates were dissolved in DMF. The concentration was determined by UV−vis absorption spectrum.

Detection of Singlet Oxygen. Generation of singlet oxygen was determined following the Kraljic procedure.[42] Solutions containing G-PLL/ZnPc, GO/ZnPc, or ZnPc (2.5, 5, 10, and 15 μM of ZnPc) were mixed with RNO (125 μM) and imidazole (125 μM) in DMF and then irradiated by 655 nm light at a power density of 65 mW/cm^2 using a LED lamp for 10 min. Generation of singlet oxygen by ZnPc or G-PLL/ZnPc would result in bleaching of RNO absorption at 440 nm, thus reflecting production of $^1O_2$.

Cellular Toxicity Assay. HeLa (a human cervical carcinoma cell line), MCF-7 (a human breast cancer cell line), and B16 (a mouse melanoma cell line) cells were all obtained from American Type Culture Collect (ATCC) and cultured in the recommended conditions. For the cytotoxicity of G-PLL, cells were seeded in 96-well plates for 24 h and treated with series concentrations of G-PLL for 24, 48, and 72 h. Then the relative cell viability was measured with cell counting kit-8 (CCK-8) (Beyotime, Shanghai, China). For the cytotoxicity of free DOX, G-PLL/DOX, free ZnPc, and G-PLL/ZnPc in the dark and under irradiation, cells were first treated with the same concentration of DOX and G-PLL/DOX (0−20 μg/mL) and ZnPc and G-PLL/ZnPc (0−10 μg/mL dissolve in DMSO and diluted in PBS) for 6 h. Then the supernatant were discarded, and the cells were washed gently with PBS 3 times and then irradiated with a 660 nm laser (BWT Beijing Ltd., Beijing, China) (0.15 W/cm^2, 10 min) for the irradiation group or no irradiation for the dark group. Following 24 h incubation, the relative cell viability was measured by CCK-8 using the cells treated with DMSO as control.

In-Vitro PDT and Chemotherapy of G-PLL/DOX/ZnPc. Cells (1×10^4 cells/well) seeded in 96-well plates were treated with series concentrations of G-PLL/DOX/ZnPc in serum-free media for 6 h. Then the supernatant were discarded, and the cells were washed gently with PBS 3 times and then irradiated with a 660 nm laser (BWT Beijing Ltd., Beijing, China) (0.15 W/cm^2, 10 min). Following 24 h incubation, the relative cell viability was measured by CCK-8.

Cellular Uptake Study by Confocal Microscopy. HeLa cells (8×10^4 cells/well) seeded in a 6-well plate were treated with G-PLL/ZnPc, G-PLL/DOX, and G-PLL/DOX/ZnPc (equivalent [ZnPc] = [DOX] = 5 μg/mL) in serum-free media for 6 h. Then the cells were fixed with paraformaldehyde (4%) for 15 min and stained with DAPI for 5 min after washing 3 times with PBS. Confocal images of cells were recorded under a Nikon ECLIPSE Ti laser scanning confocal microscope (λ_{ex} = 480 nm for DOX, 635 nm for ZnPc, 400 nm for DAPI).

Trypan Blue Staining. HeLa cells (3×10^4 cells/well) seeded in a 48-well plate were treated with G-PLL/DOX/ZnPc, G-PLL/ZnPc, and G-PLL/DOX (equivalent [ZnPc] = [DOX] = 0.625 μg/mL) in serum-free medium for 6 h. After discarding the supernatant, cells were washed with PBS 3 times and irradiated with a 660 nm laser (BWT Beijing Ltd., Beijing, China) (0.15 W/cm^2, 10 min). Then the cells were incubated for 0, 6, and 24 h. At each time point the cells were washed with PBS and stained with 0.04% trypan blue solution (Beyotime, Shanghai, China) for 3 min. Optical images of cells were then taken after washing twice with PBS.

■ ASSOCIATED CONTENT

Ⓢ Supporting Information

Synthesis and characterization of nanosized G-PLL composite, stability of G-PLL/DOX/ZnPc, G-PLL/ZnPc, and G-PLL/DOX in different solutions, and cytotoxicity of GO toward HeLa cells. This material is available free of charge via the Internet at http://pubs.acs.org.

■ AUTHOR INFORMATION

Corresponding Author

*Tel: +86-28-8320-3353, Fax: +86-28-8320-8238; E-mail: liuyiyao@hotmail.com.

Notes

The authors declare no competing financial interest.

■ ACKNOWLEDGMENTS

This research was supported by the National Natural Science Foundation of China (81101147, 81471785, 81201192, 11272083, 31470906, 31470959), China Postdoctoral Science Foundation (2011M501406), China Postdoctoral Science Special Foundation (2012T50773), Fundamental Research Funds for the Central Universities (ZYGX2011J099), Opening Research Fund from the State Key Laboratory of Bioelectronics in Southeast University, P. R. China (2011E09), and Research Start-up Grants for New Science Faculty of the University of Electronic Science and Technology of China (Y02002010901035).

■ REFERENCES

(1) Hu, C. M.; Aryal, S.; Zhang, L. Nanoparticle-assisted Combination Therapies for Effective Cancer Treatment. *Ther. Deliv.* **2010**, *1*, 323−334.

(2) Kolishetti, N.; Dhar, S.; Valencia, P. M.; Lin, L. Q.; Karnik, R.; Lippard, S. J.; Langer, R.; Farokhzad, O. C. Engineering of Self-Assembled Nanoparticle Platform for Precisely Controlled Combination Drug Therapy. *Proc. Natl. Acad. Sci. U.S.A.* **2010**, *107*, 17939−17944.

(3) Jing, L. J.; Liang, X. L.; Li, X. D.; Lin, L.; Yang, Y. B.; Yue, X. L.; Dai, Z. F. Mn-porphyrin Conjugated Au Nanoshells Encapsulating Doxorubicin for Potential Magnetic Resonance Imaging and Light Triggered Synergistic Therapy of Cancer. *Theranostics* **2014**, *4*, 858−871.

(4) Dolmans, D. E.; Fukumura, D.; Jain, R. K. Photodynamic Therapy for Cancer. *Nat. Rev. Cancer* **2003**, *3*, 380−387.
(5) Celli, J. P.; Spring, B. Q.; Rizvi, I.; Evans, C. L.; Samkoe, K. S.; Verma, S.; Pogue, B. W.; Hasan, T. Imaging and Photodynamic Therapy: Mechanisms, Monitoring, and Optimization. *Chem. Rev.* **2010**, *110*, 2795−2838.
(6) Wilson, B. C.; Patterson, M. S. The Physics, Biophysics and Technology of Photodynamic Therapy. *Phys. Med. Biol.* **2008**, *53*, R61−R109.
(7) Conte, C.; Ungaro, F.; Maglio, G.; Tirino, P.; Siracusano, G.; Sciortino, M. T.; Leone, N.; Palma, G.; Barbieri, A.; Arra, C.; Mazzaglia, A.; Quaglia, F. Biodegradable Core-shell Nanoassemblies for the Delivery of Docetaxel and Zn(II)-Phthalocyanine Inspired by Combination Therapy for Cancer. *J. Control. Release* **2013**, *167*, 40−52.
(8) Bai, D.; Xia, X.; Yow, C. M.; Chu, E. S.; Xu, C. Hypocrellin B-encapsulated Nanoparticle-Mediated Rev-Caspase-3 Gene Transfection and Photodynamic Therapy on Tumor Cells. *Eur. J. Pharmacol.* **2011**, *650*, 496−500.
(9) Lu, W.; Zhang, G.; Zhang, R.; Flores, L. G., 2nd; Huang, Q.; Gelovani, J. G.; Li, C. Tumor Site-Specific Silencing of NF-κB p65 by Targeted Hollow Gold Nanosphere-mediated Photothermal Transfection. *Cancer Res.* **2010**, *70*, 3177−3188.
(10) You, J.; Zhang, R.; Zhang, G. D.; Zhong, M.; Liu, Y.; Van Pelt, C. S.; Liang, D.; Wei, W.; Sood, A. K.; Li, C. Photothermal-chemotherapy with Doxorubicin-loaded Hollow Gold Nanospheres: A Platform for Near-infrared Light-trigged Drug Release. *J. Control. Release* **2012**, *158*, 319−328.
(11) Jang, B.; Park, J. Y.; Tung, C. H.; Kim, I. H.; Choi, Y. Gold Nanorod-photosensitizer Complex for Near-infrared Fluorescence Imaging and Photodynamic/Photothermal Therapy in Vivo. *ACS Nano* **2011**, *5*, 1086−1094.
(12) Gao, L.; Fei, J.; Zhao, J.; Li, H.; Cui, Y.; Li, J. Hypocrellin-loaded Gold Nanocages with High Two-photon Efficiency for Photothermal/Photodynamic Cancer Therapy in Vitro. *ACS Nano* **2012**, *6*, 8030−8040.
(13) Liang, X. L.; Li, X. D.; Jing, L. J.; Yue, X. L.; Dai, Z. F. Theranostic Porphyrin Dyad Nanoparticles for Magnetic Resonance Imaging Guided Photodynamic Therapy. *Biomaterials* **2014**, *35*, 6379−6388.
(14) Liang, X. L.; Li, X. D.; Yue, X. L.; Dai, Z. F. Conjugation of Porphyrin to Nanohybrid Cerasomes for Photodynamic Diagnosis and Therapy of Cancer. *Angew. Chem., Int. Ed.* **2011**, *50*, 11622−11627.
(15) Barth, B. M.; Shanmugavelandy, S. S.; Kaiser, J. M.; McGovern, C.; Altinoglu, E. I.; Haakenson, J. K.; Hengst, J. A.; Gilius, E. L.; Knupp, S. A.; Fox, T. E.; Smith, J. P.; Ritty, T. M.; Adair, J. H.; Kester, M. PhotoImmunoNanoTherapy Reveals an Anticancer Role for Sphingosine Kinase 2 and Dihydrosphingosine-1-Phosphate. *ACS Nano* **2013**, *7*, 2132−2144.
(16) Marrache, S.; Choi, J. H.; Tundup, S.; Zaver, D.; Harn, D. A.; Dhar, S. Immune Stimulating Photoactive Hybrid Nanoparticles for Metastatic Breast Cancer. *Integr. Biol.* **2013**, *5*, 215−223.
(17) Dong, H. Q.; Dong, C. Y.; Ren, T. B.; Li, Y. Y.; Shi, D. L. Surface-engineered Graphene-based Nanomaterials for Drug Delivery. *J. Biomed. Nanotechnol.* **2014**, *10*, 2086−2106.
(18) Yang, X.; Zhang, X.; Liu, Z.; Ma, Y.; Huang, Y.; Chen, Y. High-efficiency Loading and Controlled Release of Doxorubicin Hydrochloride on Graphene Oxide. *J. Phys. Chem. C* **2008**, *112*, 17554−17558.
(19) Tian, B.; Wang, C.; Zhang, S.; Feng, L.; Liu, Z. Photothermally Enhanced Photodynamic Therapy Delivered by Nano-graphene Oxide. *ACS Nano* **2011**, *5*, 7000−7009.
(20) Huang, P.; Wang, S. J.; Wang, X. S.; Shen, G. X.; Jing, L.; Wang, Z.; Guo, S. W.; Cui, D. X.; Yang, M.; Chen, X. Y. Surface Functionalization of Chemically Reduced Graphene Oxide for Targeted Photodynamic Therapy. *J. Biomed. Nanotechnol.* **2015**, *11*, 117−125.
(21) Li, F. Y.; Park, S. J.; Ling, D. S.; Park, W.; Han, J. Y.; Na, K.; Char, K. Hyaluronic Acid-Conjugated Graphene Oxide/Photosensitizer Nanohybrids for Cancer Targeted Photodynamic Therapy. *J. Mater. Chem. B* **2013**, *1*, 1678−1686.
(22) Zhou, L.; Wang, W.; Tang, J.; Zhou, J. H.; Jiang, H. J.; Shen, J. Graphene Oxide Noncovalent Photosensitizer and Its Anticancer Activity in Vitro. *Chemistry* **2011**, *17*, 12084−12091.
(23) Zhou, L.; Jiang, H.; Wei, S.; Ge, X.; Zhou, J.; Shen, J. High-efficiency Loading of Hypocrellin B on Graphene Oxide for Photodynamic Therapy. *Carbon* **2012**, *50*, 5594−5604.
(24) Zhang, L. M.; Xia, J. G.; Zhao, Q. H.; Liu, L. W.; Zhang, Z. J. Functional Graphene Oxide as a Nanocarrier for Controlled Loading and Targeted Delivery of Mixed Anticancer Drugs. *Small* **2010**, *6*, 537−544.
(25) Liu, G. D.; Shen, H.; Mao, J. N.; Zhang, L. M.; Jiang, Z.; Sun, T.; Lan, Q.; Zhang, Z. J. Transferrin Modified Graphene Oxide for Glioma-targeted Drug Delivery: in Vitro and in Vivo Evaluations. *ACS Appl. Mater. Interfaces* **2013**, *5*, 6909−6914.
(26) Chen, W. H.; Yi, P. W.; Zhang, Y.; Zhang, L. M.; Deng, Z. W.; Zhang, Z. J. Composites of Aminodextran-coated Fe_3O_4 Nanoparticles and Graphene Oxide for Cellular Magnetic Resonance Imaging. *ACS Appl. Mater. Interfaces* **2011**, *3*, 4085−4091.
(27) Miao, W.; Shim, G.; Lee, S.; Choe, Y. S.; Oh, Y. K. Safety and Tumor Tissue Accumulation of Pegylated Graphene Oxide Nanosheets for Co-delivery of Anticancer Drug and Photosensitizer. *Biomaterials* **2013**, *34*, 3402−3410.
(28) Xu, C.; Yang, D. R.; Mei, L.; Li, Q. H.; Zhu, H. Z.; Wang, T. H. Targeting Chemophotothermal Therapy of Hepatoma by Gold Nanorods/Graphene Oxide Core/Shell Nanocomposites. *ACS Appl. Mater. Interfaces* **2013**, *5*, 12911−12920.
(29) Jin, Y. S.; Wang, J. R.; Ke, H. T.; Wang, S. M.; Dai, Z. F. Graphene Oxide Modified PLA Microcapsules Containing Gold Nanoparticles for Ultrasonic/CT Bimodal Imaging Guided Photothermal Tumor Therapy. *Biomaterials* **2013**, *34*, 4794−4802.
(30) Shan, C.; Yang, H.; Han, D.; Zhang, Q.; Ivaska, A.; Niu, L. Water-soluble Graphene Covalently Functionalized by Biocompatible Poly-L-Lysine. *Langmuir* **2009**, *25*, 12030−12033.
(31) Zhang, D.; Zhang, Y.; Zheng, L.; Zhan, Y.; He, L. Graphene Oxide/Poly-L-Lysine Assembled Layer for Adhesion and Electrochemical Impedance Detection of Leukemia K562 Cancer Cells. *Biosens. Bioelectron.* **2013**, *42*, 112−118.
(32) Lin, D. W.; Bettinger, C. J.; Ferreira, J. P.; Wang, C. L.; Bao, Z. A Cell-compatible Conductive Film from a Carbon Nanotube Network Adsorbed on Poly-L-Lysine. *ACS Nano* **2011**, *5*, 10026−10032.
(33) Some, S.; Ho, S. M.; Dua, P.; Hwang, E.; Shin, Y. H.; Yoo, H.; Kang, J. S.; Lee, D. K.; Lee, H. Dual Functions of Highly Potent Graphene Derivative-Poly-L-Lysine Composites to Inhibit Bacteria and Support Human Cells. *ACS Nano* **2012**, *6*, 7151−7161.
(34) Sun, J. L.; Chao, J.; Huang, J.; Yin, M.; Zhang, H.; Peng, C.; Zhong, Z. T.; Chen, N. Uniform Small Graphene Oxide as an Efficient Cellular Nanocarrier for Immunostimulatory CpG Oligonucleotides. *ACS Appl. Mater. Interfaces* **2014**, *6*, 7926−7932.
(35) Jung, I.; Dikin, D.; Park, S.; Cai, W. W.; Mielke, S. L.; Ruoff, R. S. Effect of Water Vapor on Electrical Properties of Individual Reduced Graphene Oxide Sheets. *J. Phys. Chem. C* **2008**, *112*, 20264−20268.
(36) Liu, Z.; Robinson, J. T.; Sun, X.; Dai, H. PEGylated Nanographene Oxide for Delivery of Water-insoluble Cancer Drugs. *J. Am. Chem. Soc.* **2008**, *130*, 10876−10877.
(37) Qin, X. C.; Guo, Z. Y.; Liu, Z. M.; Zhang, W.; Wan, M. M.; Yang, B. W. Folic Acid-Conjugated Graphene Oxide for Cancer Targeted Chemo-photothermal Therapy. *J. Photochem. Photobiol., B* **2013**, *120*, 156−162.
(38) Kim, H.; Lee, D.; Kim, J.; Kim, T. I.; Kim, W. J. Photothermally Triggered Cytosolic Drug Delivery via Endosome Disruption Using a Functionalized Reduced Graphene Oxide. *ACS Nano* **2013**, *7*, 6735−6746.
(39) Kim, H. J.; Shin, K. J.; Han, M. K.; An, K.; Lee, J. K.; Honma, I.; Kim, H. One-pot Synthesis of Multifunctional Mesoporous Silica

Nanoparticle Incorporated With Zinc(II) Phthalocyanine and Iron Oxide. *Scr. Mater.* **2009**, *61*, 1137−1140.
(40) Cui, S.; Yin, D.; Chen, Y.; Di, Y.; Chen, H.; Ma, Y.; Achilefu, S.; Gu, Y. In Vivo Targeted Deep-tissue Photodynamic Therapy Based on Near-Infrared Light Triggered Upconversion Nanoconstruct. *ACS Nano* **2013**, *7*, 676−688.
(41) Lee, E. S.; Gao, Z.; Bae, Y. H. Recent Progress in Tumor pH Targeting Nanotechnology. *J. Control. Release* **2008**, *132*, 164−170.
(42) Kraljić, I.; Mohsni, E. A New Method for the Detection of Singlet Oxygen in Aqueous Solutions. *Photochem. Photobiol.* **1978**, *28*, 577−581.
(43) Zhu, Z.; Tang, Z. W.; Phillips, J. A.; Yang, R. H.; Wang, H.; Tan, W. H. Regulation of Singlet Oxygen Generation Using Single-walled Carbon Nanotubes. *J. Am. Chem. Soc.* **2008**, *130*, 10856−10857.
(44) Liu, Y. Y.; Shi, M. R.; Xu, M. M.; Yang, H.; Wu, C. H. Multifunctional Nanoparticles of Fe_3O_4@SiO_2(FITC)/PAH conjugated the Recombinant Plasmid of pIRSE2-EGFP/VEGF(165) with Dual Functions for Gene Delivery and Cellular Imaging. *Expert Opin. Drug Deliv.* **2012**, *9*, 1197−1207.
(45) Shi, M. R.; Liu, Y. Y.; Xu, M. M.; Yang, H.; Wu, C. H.; Miyoshi, H. Core/shell Fe_3O_4@SiO_2 nanoparticles Modified with PAH as a Vector for EGFP plasmid DNA delivery into HeLa cells. *Macromol. Biosci.* **2011**, *11*, 1563−1569.
(46) Chou, T. C. Theoretical Basis, Experimental Design, and Computerized Simulation of Synergism and Antagonism in Drug Combination Studies. *Pharmacol. Rev.* **2006**, *58*, 621−681.
(47) Yan, F.; Kopelman, R. The Embedding of Meta-Tetra-(Hydroxyphenyl)-Chlorininto Silica Nanoparticle Platforms for Photodynamic Therapy and Their Singlet Oxygen Production and PH-dependent Optical Properties. *Photochem. Photobiol.* **2003**, *78*, 587−591.
(48) Tang, W.; Xu, H.; Kopelman, R.; Philbert, M. A. Photodynamic Characterization and in Vitro Application of Methylene Blue-containing Nanoparticle Platforms. *Photochem. Photobiol.* **2005**, *81*, 242−249.